

# Star formation in evolving molecular clouds

M. Völschow<sup>1</sup>, R. Banerjee<sup>1</sup>, and B. Körtgen<sup>1</sup>

Hamburger Sternwarte, Universität Hamburg, Gojenbergsweg 112, 21029 Hamburg, Germany  
e-mail: marcel.voeschow@hs.uni-hamburg.de

Received 1 March 2017 / Accepted 3 July 2017

## ABSTRACT

Molecular clouds are the principle stellar nurseries of our universe; they thus remain a focus of both observational and theoretical studies. From observations, some of the key properties of molecular clouds are well known but many questions regarding their evolution and star formation activity remain open. While numerical simulations feature a large number and complexity of involved physical processes, this plethora of effects may hide the fundamentals that determine the evolution of molecular clouds and enable the formation of stars. Purely analytical models, on the other hand, tend to suffer from rough approximations or a lack of completeness, limiting their predictive power. In this paper, we present a model that incorporates central concepts of astrophysics as well as reliable results from recent simulations of molecular clouds and their evolutionary paths. Based on that, we construct a self-consistent semi-analytical framework that describes the formation, evolution, and star formation activity of molecular clouds, including a number of feedback effects to account for the complex processes inside those objects. The final equation system is solved numerically but at much lower computational expense than, for example, hydrodynamical descriptions of comparable systems. The model presented in this paper agrees well with a broad range of observational results, showing that molecular cloud evolution can be understood as an interplay between accretion, global collapse, star formation, and stellar feedback.

**Key words.** stars: evolution – stars: formation – ISM: clouds – evolution – ISM: kinematics and dynamics – ISM: structure

## 1. Introduction

Molecular clouds, the birthplaces of stars in present day galaxies, are thought to be dynamical objects continuously forming out of the diffuse interstellar medium (see, e.g., Blitz & Shu 1980). The most massive clouds may be referred to as giant molecular clouds (GMCs), but typically they contain masses between several hundred to several million solar masses, and radii of a few to a few hundred parsecs. In order to form stars, one would expect molecular clouds to feature signatures of global collapse or at least some level of local instability.

At this point, the key question that arises is: how dynamic are molecular clouds? A widely used quantity to measure global stability is the virial parameter (see, e.g., Bertoldi & McKee 1992), taking into account the mass, size, and velocity dispersion. Goldreich & Kwan (1974) argued that the linewidths observed in molecular clouds correspond to a state of global collapse. In contrast, authors such as Murray (2011) found that typical GMCs have virial parameters of order unity, that is, they roughly maintain a quasi-static equilibrium; other authors, such as McKee & Tan (2003), employed virialized cores as input for their turbulent core accretion model. Heyer et al. (2001) proposed that clouds up to  $\sim 10^4 M_{\odot}$  may be more stable, while larger clouds are subject to global collapse.

At the same time, works by Zuckerman & Evans (1974) and Zuckerman & Palmer (1974) showed that the simple picture of star formation via collapse and fragmentation of spherical clouds of cold dense gas leads to severe problems with the empirical basis. In fact, if all of our Galaxy's dense molecular gas were in free-fall, the star formation rates (SFR) would be two orders of magnitude greater than observed (see, e.g., Krumholz & McKee 2005).

Today, observed SFRs of GMCs range between  $1 M_{\odot}/\text{Myr}$  and  $1000 M_{\odot}/\text{Myr}$  (Lada et al. 2010) while canonical values for their star formation efficiency (SFE) lie in the range of a few percent for large clouds and a few tens of percent for more compact clouds (see, e.g., Krumholz & McKee 2005; Murray 2011). While small SFEs are generally attributed to large clouds and large SFEs to low-mass clouds (Krumholz & McKee 2005), no such clear mapping exists for the SFR and different levels of star formation activity are found across a broad range of molecular cloud masses and sizes (Murray 2011).

However, Palla & Stahler (2000) found that nearly all of the studied objects are the result of star formation processes that started at a low level, before a phase of steep acceleration set in. As a result, most of the stars form at the end of a molecular cloud's lifetime, which is a few ten Myrs (see, e.g., Larson 1981; Murray 2011), and we end up with age histograms that are dominated by young stars (see, e.g., Palla & Stahler 2000; Megeath et al. 2012). The impact of turbulence, magnetic fields, and the role of global collapse are still unclear, and different authors favor different pictures (see, e.g., Klessen 2000; Krumholz & McKee 2005; Hennebelle & Chabrier 2008; Zamora-Avilés et al. 2012; Körtgen & Banerjee 2015).

Evidently, the field of star formation study is still dominated by ongoing fundamental debates and has to deal with a highly inconsistent empirical basis which supports a large number of different models. A modern ansatz that potentially solves the inconsistencies between theory and observations is the hybrid picture of a dynamical interplay between gas accretion, turbulence, global collapse, star formation, and feedback (Zamora-Avilés et al. 2012).

Early studies by Wannier et al. (1983) revealed envelopes of warm atomic gas surrounding molecular clouds. These warm

gas envelopes are gravitationally bound to the molecular cloud and support continuous accretion, before feedback via winds, ionization, and supernovae (SNe) finally destroy the surrounding envelope and end accretion (see, e.g., Banerjee et al. 2009; Fukui et al. 2009), naturally limiting the cloud's lifetime.

Large clouds may further suffer from so-called fragmentation-induced starvation, limiting accretion onto individual stars and small stellar systems, and limiting the efficiency of star formation processes to the values we observe today (see, e.g., Peters et al. 2010a; Girichidis et al. 2012). Colliding flows of galactic gas are a straightforward explanation for the formation of gravoturbulent molecular clouds as they can initiate a phase transition from warm neutral gas to the cold neutral medium which has been studied intensively both numerically and theoretically (see, e.g., Hennebelle & Péroul 1999; Koyama & Inutsuka 2000; Vázquez-Semadeni et al. 2006). Vázquez-Semadeni (1994) found that a lognormal distribution resembles the distribution of densities under isothermal gravoturbulent conditions which are indeed met in molecular clouds (see, e.g., Padoan & Nordlund 2002; Krumholz & McKee 2005; Hennebelle & Chabrier 2008). Observational studies by Schneider et al. (2013, 2015) proved that such a lognormal distribution of densities fits the observed density structure of GMCs very well, both in the solar neighborhood and towards the galactic center (see Rathborne et al. 2014). More specifically, a work by Klessen (2000) supported by recent observations (see, e.g., Schneider et al. 2015) and additional theoretical work (see, e.g., Federrath & Klessen 2012, 2013; Girichidis et al. 2014) revealed the presence of a power-law tail at the high-mass end of the density distribution as an indicator of ongoing star formation processes.

Based on these recent findings, we propose a self-consistent dynamical model to describe the full evolution of molecular clouds on all scales via a set of analytical expressions. The model only depends on a small number of simple physical and astrophysical quantities frameworked by recent advances in how molecular clouds evolve, testing whether all these individual results can add up to one consistent model. In fact, our model is able to describe a large set of observations adequately and predicts a number of new effects that call for observational verification. The structure of our paper is as follows: first, we start with the most important factor and describe how gas is transformed into stars. In the next section, we elaborate on the analytical framework describing how gas is accreted from surrounding HI streams and converted into a molecular cloud that evolves over time. Next, we explain our implementation of stellar feedback before we present and discuss the full model results.

## 2. From gas to stars

The main ingredient of any cloud model is how the dense parts of the cloud's density distribution are transformed into stars. Typically, the lognormal probability density function (PDF) as found in gravoturbulent molecular clouds is expressed in terms of the normalized logarithmic density coordinate  $s := \log(\rho/\rho_0)$  with mean density of the cloud  $\rho_0$ . In this coordinate system, the canonical form of the volume-weighted PDF of density fluctuations is

$$P_V(s) = \frac{1}{\sqrt{2\pi}\sigma^2} \exp\left(-\frac{(s-s_0)^2}{2\sigma^2}\right), \quad (1)$$

with  $s_0 = -1/2\sigma^2$  (see, e.g., Vázquez-Semadeni et al. 2010) and a turbulence-dependent width  $\sigma$  given by

$$\sigma^2 = \ln(1 + b^2 \mathcal{M}^2), \quad (2)$$

where  $\mathcal{M}$  is the thermal Mach number (see, e.g., Padoan & Nordlund 2002; Federrath et al. 2010). The parameter  $b$  accounts for the type of turbulence (see Federrath et al. 2008). Vázquez-Semadeni et al. (2010) set it to unity. Regarding the turbulent Mach number, we follow Heiles & Troland (2003) who showed that the coldest and densest parts of the interstellar medium (ISM) have typical mean Mach numbers of three which we will use whenever explicit calculations are in order. Further, we impose a constant mean Mach number over the entire cloud evolution time, neglecting possible energy and momentum by supernovae, winds, and outflows (see, e.g., Banerjee et al. 2007; Rogers & Pittard 2013; Bally 2016; Padoan et al. 2016). The PDF is normalized to

$$\int_s^\infty ds s P_V(s) = 1. \quad (3)$$

### 2.1. SFR and SFE

Formally, the instantaneous mass in stars  $M_S(t)$  is related to the star formation rate  $SFR(t)$  via:

$$M_S(t) = \int_0^t SFR(t') dt'. \quad (4)$$

Stars form out of collapsing fragments in the cold and dense parts of the cloud. Krumholz & McKee (2005) found that the star formation rate is determined by the mass fraction of cold and dense gas over the free-fall time of the cloud, which is  $t_{\text{ff}} = \sqrt{3\pi/32G\mu m_{\text{H}}n}$  in the spherical case or  $t_{\text{ff}} = \sqrt{R_C/2h_C G\mu m_{\text{H}}n}$  with cloud radius and height  $R_C$  and  $h_C$  for cylindrical sheets (Toalá et al. 2012). Using that, we can write the instantaneous star formation rate as

$$SFR(t) = \frac{M_{\text{thresh}}}{t_{\text{ff}}} = \frac{M_C f}{t_{\text{ff}}}, \quad (5)$$

where  $M_{\text{thresh}}$  is the star-forming mass fraction and  $f$  denotes the fraction of the cloud's dense gas mass  $M_C$  that goes into stars.

Calculating  $M_{\text{thresh}}$  is the key aspect of this work. Different star formation criteria have been put forward in the literature to calculate the fraction of star-forming mass  $f$  (see, e.g., Padoan & Nordlund 2002; Krumholz & McKee 2005; Hennebelle & Chabrier 2008). We shall start with our new approach: a revised version of the (Padoan 1995) formalism. Our description closely follows Banerjee (2014).

### 2.2. Star formation criteria

#### 2.2.1. The core-mass function formalism

From observations, the distribution of stellar cores (core-mass function CMF) is known to follow a Salpeter power law of the form

$$\text{CMF} = \frac{dN}{d\log M} = C M^{-\alpha}, \quad (6)$$

with normalization constant  $C$  and slope  $\alpha$  (see, e.g., Salpeter 1955; Lada et al. 2008; Rathborne et al. 2009).

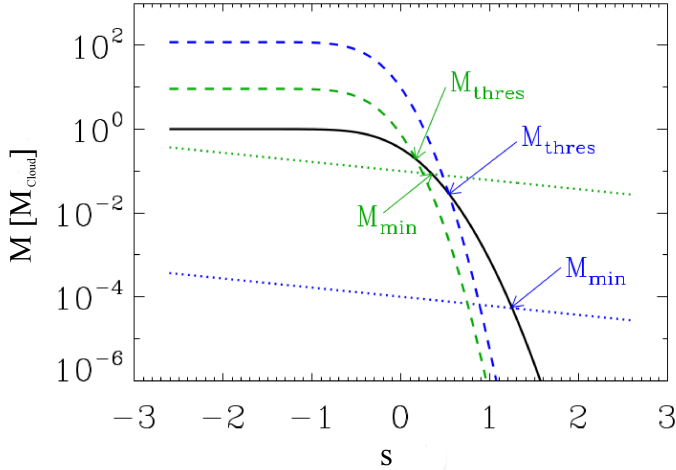


**Fig. 1.** Illustration of the CMF formalism as described in Sect. 2.2.1. The density of the lowest possible core can be interpreted as the intersection of the cumulated density PDF (black line) and the Jeans mass (dotted lines) which has a constant slope in this log-log plot. The dashed lines are the normalized Salpeter core-mass functions and their intersection with the cumulated density PDF equals the lower density threshold.  $M_{\text{thresh}}$  is the total mass that will be transformed into stars.

The smallest core that can be formed out of the cloud gas can be illustrated as a sphere of all the densest parts of the cloud cumulated into one single object, starting from a density threshold  $s_{\text{min}}$  and ranging to infinity. The core collapses once its mass exceeds a Jeans mass  $M_J(s_{\text{min}})$ . We can find this minimal core by solving

$$\frac{M_C}{2} \left[ 1 - \operatorname{erf} \left( -\frac{s_{\text{min}} - \sigma^2/2}{\sqrt{2}\sigma} \right) \right] = M_J(s_{\text{min}}), \quad (7)$$

where  $M_C$  is the cloud mass. The minimal core mass can be found by integrating the dense parts of the PDF up to a density  $s_{\text{min}}$  where the total integrated mass exceeds a Jeans mass  $M_J(s_{\text{min}})$ . Such a minimal core of mass  $M_J(s_{\text{min}}) = M_{\text{min}}$  defines the high-mass end of the CMF. The CMF normalization parameter is determined via the total mass of the cloud:

$$\int_{M_{\text{min}}}^{M_C} dM M^{-\alpha} = C \frac{M_{\text{min}}}{\alpha - 1}. \quad (8)$$

The normalized CMF can be used to calculate the number of cores within a mass range starting from an arbitrary mass threshold  $M$  up to the cloud mass via

$$\begin{aligned} N(M) &= C \int_M^{M_C} dM M^{-\alpha-1} \\ &= \frac{\alpha - 1}{\alpha} \left( \frac{M_C}{M_{\text{min}}} \right) \left[ \left( \frac{M}{M_{\text{min}}} \right)^{-\alpha} - \left( \frac{M_C}{M_{\text{min}}} \right)^{-\alpha} \right]. \end{aligned} \quad (9)$$

Using the equation above, we can define a threshold mass by imposing that the mass fraction between  $M_{\text{thresh}}$  and  $M_C$  (see Fig. 1) be at least one cloud which, in a hierarchical cloud picture, is the largest cloud that contains all other cores (see, e.g., Vázquez-Semadeni et al. 2006). This implies that we have to solve

$$N(M_{\text{thresh}}) = 1 \quad (10)$$

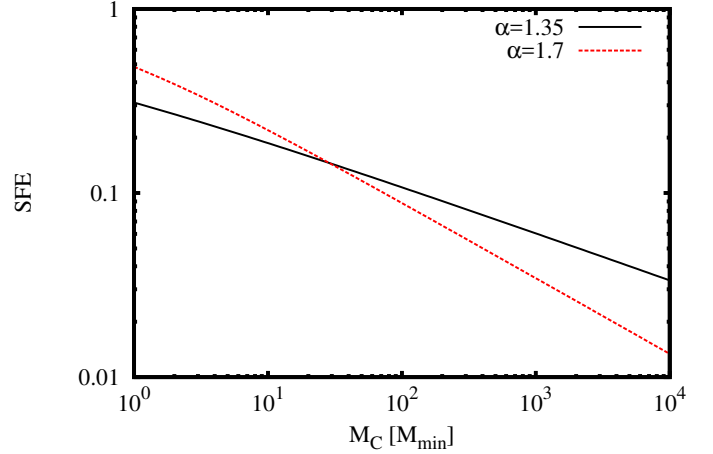


**Fig. 2.** Star formation efficiency, as defined in Sect. 2.2.1 as a function of the cloud mass to minimal core mass ratio  $M_C/M_{\text{min}}$ . Smaller clouds have a typical SFE exceeding 10% while bigger clouds transform gas into stars less efficiently.

for  $M_{\text{thresh}}$  (see Fig. 1). After a few manipulations, we arrive at a total star-forming mass of

$$M_{\text{thresh}} = M_{\text{min}} \left( \frac{\alpha}{\alpha - 1} \frac{M_{\text{min}}}{M_C} + \left( \frac{M_{\text{min}}}{M_C} \right)^{\alpha} \right)^{-1/\alpha}, \quad (11)$$

where a typical value for  $\alpha$  is given by 1.35 (see, e.g., Lada et al. 2008). Using this mass, we can calculate the instantaneous SFR as given by Eq. (5) and define an instantaneous star formation efficiency  $SFE = M_{\text{thresh}}/M_C$  or

$$SFE = \left[ \left( \frac{\alpha}{\alpha - 1} \right) \left( \frac{M_C}{M_{\text{min}}} \right)^{-1} + \left( \frac{M_C}{M_{\text{min}}} \right)^{-\alpha} \right]^{-1/\alpha} \left( \frac{M_C}{M_{\text{min}}} \right)^{-1}. \quad (12)$$

Interestingly, the SFE only depends on the slope of the core-mass function and the cloud-core ratio  $M_C/M_{\text{min}}$ . In Fig. 2 we plotted the SFE as a function of the cloud-core ratio for two different CMF slopes. While massive clouds are expected to have SFEs in the range of a few percent, small clouds are much more efficient at forming stars. Compared to the Krumholz & McKee (2005) criterion, our formalism does not depend on a set of efficiency factors determined via simulations. Instead, the only input parameters are the density PDF and the slope of the core-mass function.

### 2.2.2. Constant density threshold

A number of authors argue that all mass beyond a specific constant density threshold is transformed into stars (see, e.g., Krumholz & McKee 2005; Zamora-Avilés et al. 2012). From the observer's side, the idea that star formation takes place in the densest parts of the cloud is a well-established fact and authors such as Lada et al. (2009) or Howard et al. (2014) give typical densities of star forming regions (clumps) in the order of  $n_{\text{thresh}} \approx 10^4 \text{ cm}^{-3}$  and above. Explicitly, for a given star formation density threshold

$$s_{\text{thresh}} = \ln \left( \frac{n_{\text{thresh}}}{n_0} \right), \quad (13)$$

the fraction of mass that goes into stars can be written as

$$f = \frac{1}{2} \left[ 1 - \operatorname{erf} \left( -\frac{s_{\text{thresh}} - \sigma^2/2}{\sqrt{2}\sigma} \right) \right], \quad (14)$$

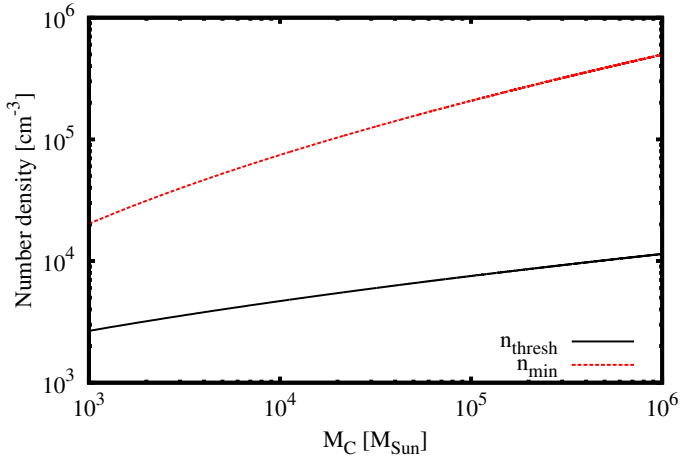


**Fig. 3.** Minimal core density and star formation threshold density for a cloud with a mean density of  $100 \text{ cm}^{-3}$  and varying mass. For a given cloud, all mass between those two thresholds will be converted into stars.

assuming a log-normal PDF. While authors such as Zamora-Avilés et al. (2012) fitted  $s_{\text{thresh}}$  to resemble numerical results, Krumholz & McKee (2005) derived

$$s_{\text{thresh}} = 1.07 \mathcal{M}_{\text{rms}}^2 \quad (15)$$

where  $\mathcal{M}_{\text{rms}}$  denotes the turbulent Mach number of the cloud. Authors such as Zamora-Avilés et al. (2012) found ranges between  $10^5 \text{ cm}^{-3}$  and  $10^7 \text{ cm}^{-3}$  as best-fit solutions but employed a different definition of the SFR that incorporates the local core free-fall time rather than the global cloud free-fall time. Observations tend to threshold values in the range of  $10^4 \text{ cm}^{-3}$  to  $10^5 \text{ cm}^{-3}$  (see, e.g., Pudritz & Kevlahan 2013; Howard et al. 2014). Studies of molecular clouds in the galactic center show increased star formation threshold densities which do not support the idea of a single universal density threshold (see, e.g., Kruijssen et al. 2014). Furthermore, the constant-density criterion shows purely positive scaling for increasing cloud turbulence (cf. Fig. 5), contrary to findings by authors such as Krumholz & McKee (2005). On top of that, the total mass beyond such extremely high density thresholds may even be smaller than a single thermal Jeans mass. The differences between the three criteria presented here are the subject of the next subsection.

### 2.3. Comparing different star formation criteria

#### 2.3.1. Threshold and core densities

In what follows, we calculate typical star formation threshold densities and minimal core densities in the CMF formalism for a set of different clouds. Figure 3 shows the star formation threshold densities and minimal core densities for clouds of masses between  $10^2 M_{\odot}$  and  $10^6 M_{\odot}$ , all with a mean density of  $100 \text{ cm}^{-3}$  and a molecular weight  $\mu = 2.35$ . We assumed  $\mathcal{M} = 3$  for all clouds. For the typical mass and density range presented in Fig. 3, the minimal core densities lie between  $10^5 \text{ cm}^{-3}$  and  $10^8 \text{ cm}^{-3}$ . The SF threshold densities vary between  $10^3 \text{ cm}^{-3}$  and  $10^6 \text{ cm}^{-3}$  for extremely dense and massive clouds bracketing the typical star formation threshold densities found in the literature (see Sect. 2.2.1).

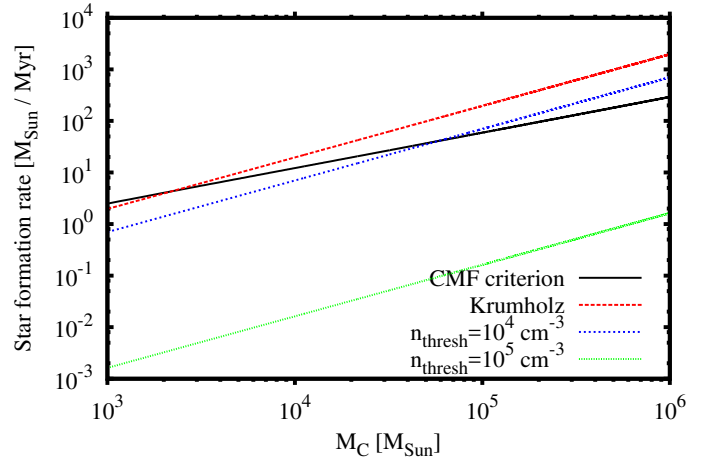


**Fig. 4.** Star formation rates for a cloud with a mean density of  $100 \text{ cm}^{-3}$  and varying mass, calculated with different star formation criteria: the CMF formalism, the Krumholz & McKee (2005) formalism, and two constant-threshold criteria. In the high-threshold case ( $10^5 \text{ cm}^{-3}$ ), virtually no stars are formed even for massive clouds while all other criteria yield comparable SFRs and show similar scaling.

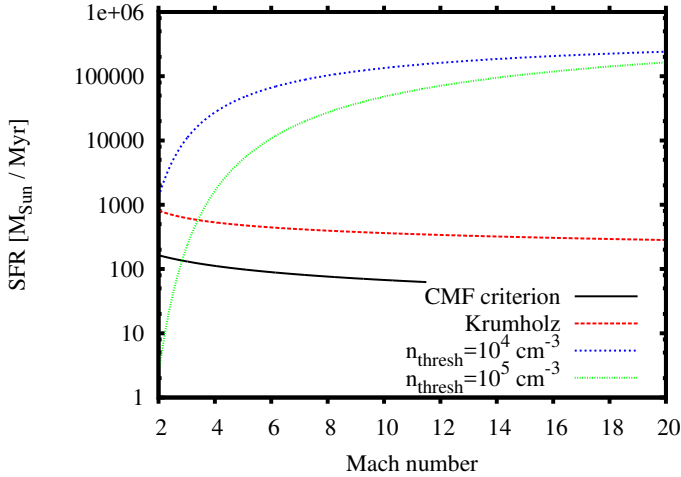
#### 2.3.2. Star formation rates and efficiencies

Figure 4 shows the star formation rate for clouds of varying mass and identical mean density of  $100 \text{ cm}^{-3}$ , comparing the CMF formalism and different constant threshold density criteria. We assumed  $\mathcal{M} = 3$  for all clouds. In Fig. 4, the star formation rates given by the different star formation criteria spread over eight orders of magnitude. The CMF criterion, the Krumholz & McKee (2005) formalism, and the low-density threshold predict similar star formation rates and show comparable scaling. On the other hand, for the  $10^5$  threshold criterion we expect almost no star formation with star formation rates far below  $1 M_{\odot}/\text{Myr}$ , conflicting with observational results for such low-mass molecular clouds which are indeed actively forming stars (see, e.g., Murray 2011).

#### 2.3.3. The impact of turbulence

In Fig. 5, we selected a cloud with intermediate properties, that is, a density of  $10^3 \text{ cm}^{-3}$  and a mass of  $10^5 M_{\odot}$ , and varied the mean Mach number of the cloud to work out the impact of turbulence on the star formation rate. As expected, the constant-threshold criteria predict higher star formation rates for increasing Mach numbers. This result represents the fact that higher Mach numbers lead to a broader PDF with more mass at lower and higher densities. The effect is dramatic: for the high-threshold criterion, the star formation rate increases by three orders of magnitude if we increase the Mach number from 2 to 6, that is, by half a magnitude. The lower thresholds react less sensitively to Mach number variations but still, constant threshold density star formation criteria are sensitive to changes in the cloud's mean Mach number, with a purely positive feedback on the star formation rate.

In contrast, the CMF criterion shows almost no variation of the star formation rate for increasing Mach numbers, with just a weakly negative trend resulting from the broadening of the PDF for increasing Mach numbers. However, beyond a Mach number of 11, Eq. (10) has no solution and the SFR drops to zero. Hence, the CMF criterion predicts that star formation is terminated beyond a critical Mach number (see Fig. 6). Below,



**Fig. 5.** Turbulence dependence of the star formation rate for an intermediate cloud with mean density  $10^3 \text{ cm}^{-3}$  and mass  $10^5 M_\odot$ . Constant threshold density models are very sensitive to changes in the cloud’s global Mach number with a clearly positive trend for increasing Mach numbers. On the other hand, the star formation rate as calculated via the CMF formalism scales just weakly with the Mach number and gives results similar to the [Krumholz & McKee \(2005\)](#) criterion. Both criteria show opposite scaling: additional turbulence decreases star formation rates. As explained in Sect. 2.3.3, in the CMF formalism star formation is terminated beyond a certain Mach number threshold.

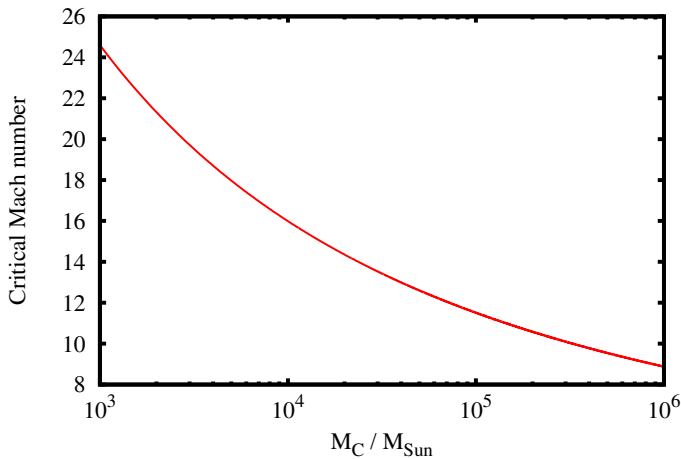


**Fig. 6.** Critical Mach number as a function of the cloud’s mass for a cloud with mean density  $10^3 \text{ cm}^{-3}$ . Smaller clouds continue their star formation activity even for very high Mach numbers, while larger clouds with more than a few  $10^5 M_\odot$  terminate below Mach 10.

the CMF criterion and the [Krumholz & McKee \(2005\)](#) threshold show similar scaling and differ only by half a magnitude.

### 3. Cloud evolution

In what follows, we describe a full dynamical model framework inspired by [Zamora-Avilés et al. \(2012\)](#) covering accretion, contraction, star formation, and feedback in which we implemented the CMF star formation criterion.

#### 3.1. Model framework

Let us assume that the gaseous part of the cloud ( $M_C$ ) follows a mass budget equation of the form

$$M_C(t) = M_A(t) - M_S(t) - M_F(t). \quad (16)$$

The cloud accretes gas  $M_A$  which increases its gas content, while formation of stars  $M_S$  and feedback effects ( $M_F$ ) may decrease the gas content again. The most fundamental process in the formation of a molecular cloud is accretion from the surrounding medium via gas streams or HI envelopes (see, e.g., [Vázquez-Semadeni et al. 2006](#); [Fukui et al. 2009](#)).

#### 3.2. Accretion

Assuming that the cloud’s geometrical radius  $R_C$  defines its cross-section for the accretion process and the cloud is fed by two streams, the mass infall rate is given by

$$\dot{M}_{\text{inf}}(t) = 2 \rho_{\text{inf}} v_{\text{inf}} (\pi R_C^2), \quad (17)$$

with infall gas density  $\rho_{\text{inf}}$  and gas velocity  $v_{\text{inf}}$  (see [Zamora-Avilés et al. 2012](#)), where the mass density  $\rho$  is linked to the number density  $n$  via  $\rho_{\text{inf}} = n_{\text{inf}} \mu_{\text{H}}$  with mean molecular weight  $\mu$ . As our model focuses on the evolution of the cold medium and does not cover the details of the transformation from atomic to molecular gas, we require the cloud to be shielded against the ambient UV flux. Given the initial mean density of the cloud of  $100 \text{ cm}^{-3}$  and the size of the smallest clouds we consider (a few pc), typical shielding column densities are well exceeded (see, e.g., [Franco & Cox 1986](#)). The instantaneous accreted mass now reads

$$M_A(t) = \int_0^t \dot{M}_{\text{inf}}(t') dt', \quad (18)$$

where we assume that the warm gas from the streams is directly converted into molecular gas  $M_C$ . Out of this molecular cloud gas, stars form as given by Eq. (5) where we calculate the fraction of mass that goes into stars using our CMF criterion (cf. Sect. 2.2.1). In addition, following [Zamora-Avilés et al. \(2012\)](#) we define an instantaneous star formation efficiency

$$SFE = \frac{M_S}{M_{\text{Acc}}}, \quad (19)$$

as the mass in stars over the total accreted stream gas mass, that is, mass in dense gas, diffuse gas, and stars.

Throughout the evolution, we keep the initial cloud radius as accretion radius accounting for gravitational focussing. This model does not depend on a colliding flow scenario but for the moment we keep the comprehensive picture of two feeding streams. Furthermore, we did not account for accretion flow feedback which can terminate the accretion of new material for weak accretion flows (see, e.g., [Peters et al. 2010a](#)).

#### 3.3. Global evolution

For the colliding streams scenario, [Vázquez-Semadeni et al. \(2006\)](#) found that a cloud’s global evolution can be divided up into two stages:

- Accretion stage: the cloud only grows in height at a constant radius and constant density until it becomes Jeans-unstable.
- Contraction stage: the cloud’s density and height remain approximately constant, but radial contraction sets in. As a result, the cloud’s radius decreases and its mean density increases.

During the two evolutionary stages, different boundary conditions for the cloud’s evolution hold.

### 3.3.1. Accretion stage

Initially, the cloud only grows in height while maintaining a constant mean density of  $n_0 = 10^2 \text{ cm}^{-3}$  and constant cloud radius  $R_C = R_{\text{inf}}$ , that is, it equals the inflow radius. Under such boundary conditions, the identity

$$M_C(t) = \rho_{\text{inf}} \pi R_C^2 h(t) \quad (20)$$

applies which can be solved for the cloud's height  $h(t)$ . The mass accretion stage ends once the cloud exceeds its thermal Jeans mass. For a finite and isothermal sheet of gas, [Larson \(1985\)](#) gives a Jeans mass of

$$M_J = 4.67 \frac{\pi R_C^2 c_s^4}{G^2 M_C}, \quad (21)$$

where  $c_s$  denotes the mean speed of sound of the cloud, which is given by  $c_s = \sqrt{k_B T_C / \mu m_H}$  with Boltzmann constant  $k_B$ , mean cloud temperature  $T_C$ , mean molecular weight  $\mu$  of the cloud, and hydrogen mass  $m_H$ . Following [Zamora-Avilés et al. \(2012\)](#) with a given initial mean density of  $100 \text{ cm}^{-3}$ , the cooling function provided by [Koyama & Inutsuka \(2002\)](#) gives a mean cloud temperature of  $T_C = 42 \text{ K}$ , constant throughout the accretion phase. Once the cloud exceeds its Jeans limit, the transition to the contraction stage occurs.

### 3.3.2. Contraction stage

During the contraction stage, the cloud maintains its height and starts to contract radially. Following [Vázquez-Semadeni et al. \(2010\)](#) and [Zamora-Avilés et al. \(2012\)](#), we use a coordinate system with origin in the center of the cloud and  $x$ -direction defined by one of the inflows. In this reference frame, we calculate the self-gravity of the cloud by integrating over mass elements  $\bar{\rho} dx dy dz$  summing up to a gravitational acceleration of

$$a(t) = G\bar{\rho} \int_{-R_C}^{+R_C} dz \int_0^{\sqrt{R_C^2 - z^2}} dy \int_{-h/2}^{h/2} \frac{R_C - z}{[(R_C - z)^2 + y^2 + x^2]^{3/2}} dx. \quad (22)$$

The first and second integral can be solved analytically. Finally, we arrive at

$$a(t) = 2G\bar{\rho} \int_{-R_C}^{+R_C} dz \arctan \left( \frac{h \sqrt{R_C^2 - z^2}}{(R_C - z) \sqrt{h^2 + 8R_C(R_C - z)}} \right). \quad (23)$$

This integral is solved numerically using the Simpson rule and the new cloud radius is calculated as described in [Zamora-Avilés et al. \(2012\)](#).

For a real cloud, collapse is usually not in pure free-fall as thermal, magnetic, and turbulent pressure counteract gravity. In order to account for that, [Zamora-Avilés et al. \(2012\)](#) introduced a correction factor  $f_L$  based on Larson's work on molecular cloud collapse which found that typical collapse times are slower by a factor of 1.58. Furthermore, we assume that the streams are gravitationally focussed onto the cloud, keeping the accretion radius and rate constant throughout the simulation.

### 3.4. Mass function evolution

In our model, we assume that every fraction of stars  $\Delta M$  formed at a given timestep  $\Delta t$  follows a Kroupa initial mass function

(IMF). Typical lifetimes can be calculated using

$$\tau \simeq 10^{10} \text{ yr} \left( \frac{M}{M_\odot} \right)^{-\alpha}, \quad (24)$$

with  $\alpha \approx 3-4$ , where we adopt 3.5 (see [Adams & Laughlin 1997](#)). This allows for explicit calculation of the shape of the stellar mass function which is crucial for the calculation of the feedback effects as carried out in the next section.

## 4. Stellar feedback

### 4.1. Stellar wind

In the recent literature, two contradicting positions are represented regarding the role of stellar wind and its impact on star formation: no impact versus large impact. Authors such as [Ngoumou et al. \(2014\)](#) studied the impact of a massive O7.5 star on stellar cores and found that stellar winds have only modest direct effects on star formation and the density distribution. Instead, low and intermediate density gas shows the most significant modulations, but as it does not contribute to the star formation processes, [Ngoumou et al. \(2014\)](#) conclude that the global impact of stellar winds on star formation is modest.

[Rogers & Pittard \(2013\)](#) studied the feedback effects of three massive stars embedded in a  $3240 M_\odot$  molecular cloud. Consistently, they found that coupling between the stellar wind and the molecular material is weak. By the end of the lifetime of massive stars, just a small fraction of the molecular cloud is pushed out of the simulation box, following paths of least resistance through the porous gas. Overdense regions remained largely unaffected.

[Dale et al. \(2014\)](#) studied the combined effects of ionization and stellar winds and found that overall star formation efficiencies are reduced just by 10–20%. According to them, the main effect of stellar winds is the creation of cavities with radii of several parsecs which modulate the efficiency of consecutive feedback processes. Low-mass clouds are more affected.

In contrast to the work mentioned previously, newer results by [Fierlinger et al. \(2016\)](#) re-emphasize the importance of stellar winds. In extensive 1D studies of the energy retained in the surrounding molecular cloud, the authors found that wind-blown cavities reduce radiative losses of subsequent supernovae and may increase the retained energy and thus the feedback efficiency. In general, the energy injected by stellar winds and by supernovae are of comparable orders of magnitude.

In conclusion, stellar winds and their interaction with molecular material are still not fully understood and all studies presented here have limitations in terms of neglected processes, limited resolution, or size of the cloud and cluster. For the moment, we follow authors such as [Rogers & Pittard \(2013\)](#), [Dale et al. \(2014\)](#), and [Ngoumou et al. \(2014\)](#) and neglect the impact of stellar winds.

### 4.2. Ionization

An approximative treatment of ionization was proposed by [Zamora-Avilés et al. \(2012\)](#): the authors calculated the mass of a representative typical massive star, that is, the mean mass of the Kroupa IMF in the range  $[8, 60] M_\odot$ , which is  $\langle M_{\text{OB}} \rangle = 17 M_\odot$  with its corresponding Lyman flux of  $\bar{S}_* = 2 \times 10^{48} \text{ s}^{-1}$ , and applied this flux to the total number of massive stars. In our model, we assume that the gravoturbulent conditions and the constant mass inflow allow for efficient recombination. Hence, the total

ionized mass is given by the gas inside all massive stars' Stroemgren spheres, that is,

$$R_{\text{HII},0} = \left( \frac{3 \bar{S}_*}{4\pi \alpha_{\text{H}}^* \bar{n}^2} \right)^{1/3}. \quad (25)$$

Here,  $\bar{S}_*$  denotes the star's ultraviolet (UV) flux,  $\alpha_{\text{H}}^*$  is the hydrogen recombination coefficient, and  $\bar{n}$  the mean number density of the cloud. Following Zamora-Avilés et al. (2012) and assuming a gas temperature inside the HII regions of  $10^4$  K, we have a recombination coefficient of  $\alpha_{\text{H}}^* = 2.6 \times 10^{-13} \text{ cm}^{-3} \text{ s}$  and arrive at typical Stroemgren radii in the range of a parsec. Over time, the heated HII bubbles expand into the molecular material which can be described via

$$R_{\text{HII}} = R_{\text{HII},0} \left( 1 + \frac{7 c_{\text{HII}} t}{4 R_{\text{HII},0}} \right)^{4/7} \quad (26)$$

(see Spitzer 1978). The sound speed in HII regions  $c_{\text{HII}}$  is calculated assuming a gas temperature of  $10^4$  K and  $\mu = 0.5$ . For the age of the HII region  $t$  we calculate the mean age of all massive stars that formed up to the given time. In order to account for the expected amount of overlap between the HII regions, we assume an equal 2D distribution of the (massive) stars in the  $y$ - $z$  plane and apply an overlap correction factor of the form

$$M_{\text{ion}} = M_{\text{C}} [1 - \exp(-\beta N_{\text{HII}})], \quad (27)$$

where  $\beta$  is a function of  $\xi = R_{\text{HII}}/R_{\text{C}}$ . In extensive simulations of clouds with a varying number of equally-sized HII regions, we calculated the mean fractional area covered by HII regions. We find that  $\beta = 0.830865 \xi^{2.01978}$  fits the simulated data well.

### 4.3. Supernovae

Massive stars beyond a certain mass threshold (typically  $8 M_{\odot}$ ) end their life with a core-collapse supernova inserting typical energies of  $10^{51}$  erg in a short period (see, e.g., Körtgen et al. 2016). The expanding shockwave destroys molecular material, potentially affecting star formation processes as well as the global gas dynamics. Authors such as Rogers & Pittard (2013) studied the impact of supernovae on a molecular environment and found that the expanding supernova shockwave indeed destroys the molecular material it bypasses within a radius of several parsecs, but does not fully evacuate the affected region because of weak coupling. Rather, the heated material may cool quickly and re-form molecular gas if gas dynamics allow for efficient cooling and transport. As a result, more than 99% of the supernova energy may escape the cloud (Rogers & Pittard 2013).

Based on these findings, we do not expect supernovae to influence the global dynamics of our cloud, that is, the global mean Mach number or the distribution of densities. Thus, we limit the effect of supernova explosions to the destruction of molecular gas within a radius of  $R_{\text{SN}} = 5$  pc consistent with typical cooling timescales of  $10^3$  yr and shockwave velocities  $\sim 10^4 \text{ km s}^{-1}$  (see Rogers & Pittard 2013) and with results by Körtgen et al. (2016) and Wareing et al. (2017). The SN frequency is calculated self-consistently using the number of massive stars that left the main sequence. Again, a statistical overlap correction is applied (see Sect. 4.2).

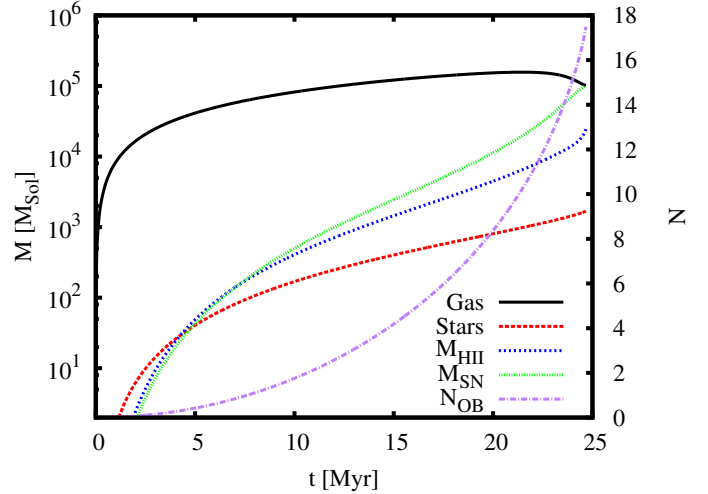


**Fig. 7.** Temporal evolution of a typical cloud. Here, we selected  $R_0 = 64$  pc as an example setup and plotted the evolution of the gas content and stellar content, as well as the amount of gas destroyed via ionization and supernova feedback.

## 5. Full model parameter study

In the previous sections, we derived all the building blocks necessary to set up our full model in which we incorporated the CMF star formation criterion as described in Sect. 2.2.1. In what follows, we present an overview of our simulations for clouds with varying initial radii. The parameters we use are summarized in Table 1. Every cloud's evolution was tracked until it either dropped below a radius of 1 pc, exceeded a mean density of  $10^6 \text{ cm}^{-3}$ , or lost more than 99% of its mass by feedback processes.

### 5.1. Temporal evolution

Before we show and discuss the results of our full parameter study, we shall start with the temporal evolution of one generic cloud to illustrate a common evolutionary path. As a working example, we chose  $R_0 = 64$  pc (see Fig. 7). The cloud continuously accretes mass from the streams, leading to an increasing gas content. As a result, stars form at initially very low rates  $< 10 M_{\odot}/\text{Myr}$  but with a clearly accelerating trend. Consequently, the stellar content increases and so do the feedback effects. Initially, feedback via SNe and ionization are of comparable effect but the second half of the cloud's lifetime is clearly dominated by SN feedback. Finally, SN feedback disrupts the cloud and star formation is terminated. Compared to the Zamora-Avilés et al. (2012) model on which we based our work, feedback builds up much more slowly and is less dominant, leading to higher cloud masses (their Fig. 2). As a consequence of both our lower overall feedback efficiency and our higher fiducial flow velocity, the lifetime of our cloud is reduced as is the final stellar content.

### 5.2. Peak gas and star masses

In Fig. 8 we present four peak masses as functions of the initial cloud radius: gas and stellar content as well as the peak ionized mass and mass destroyed by supernovae. All four quantities scale clearly positively with initial cloud radius. Supernova feedback is the dominating feedback process, only for small clouds and during the first half of the cloud lifetime is ionization of

**Table 1.** Summary of parameters used throughout all calculations.

Name	Symbol	Value	Unit
Salpeter core-mass function slope (linear)	$\alpha$	2.35	–
Hydrogen recombination coefficient	$\alpha_{\text{H}}^*$	$2.6 \times 10^{-19}$	$\text{s}^{-1}$
Larson parameter	$f_{\text{L}}$	1.7	–
Kroupa IMF lower limit	$M_{\text{Kroupa,min}}$	0.01	$M_{\odot}$
Kroupa IMF upper limit	$M_{\text{Kroupa,max}}$	60	$M_{\odot}$
Cloud mean molecular weight	$\mu_{\text{C}}$	2.35	–
Inflow mean molecular weight	$\mu_{\text{inf}}$	1.27	–
Cloud mean Mach number	$M_{\text{rms}}$	3	–
Inflow number density (initial cloud density)	$n_{\text{CNM}} = n_0$	100	$\text{cm}^{-3}$
Supernova ionization radius	$R_{\text{SN}}$	5	pc
Inflow velocity	$v_{\text{inf}}$	10	$\text{km s}^{-1}$
Cloud temperature	$T_{\text{C}}$	42	K

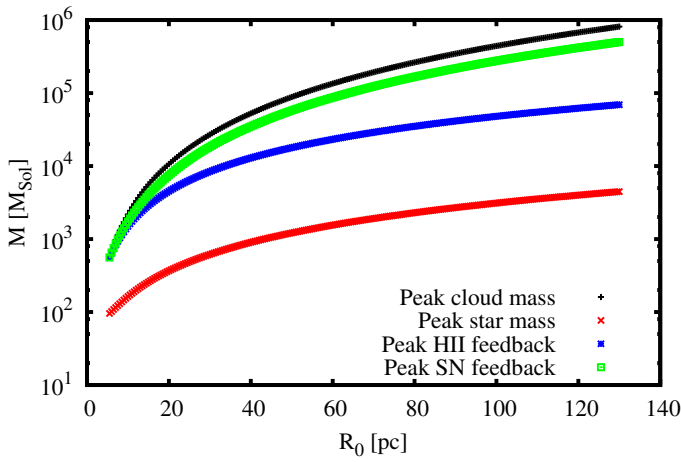


**Fig. 8.** Peak gas mass, star mass, and mass destroyed via feedback processes for clouds with varying initial radii. Throughout the parameter range, larger initial cloud and accretion stream radii lead to larger peak gas masses, an increased stellar content, and a higher fraction of mass destroyed by feedback processes. The peak gas mass and star mass follow simple power laws.

a comparable order of magnitude. Specifically, we find that the peak gas mass can be described with a generic power law of the form

$$\frac{\hat{M}_{\text{C}}}{M_{\odot}} \simeq 10 \left( \frac{R_0}{\text{pc}} \right)^{2.3}, \quad (28)$$

while the peak star mass follows

$$\frac{\hat{M}_{\text{S}}}{M_{\odot}} \simeq 6.0 \left( \frac{R_0}{\text{pc}} \right)^{1.4}, \quad (29)$$

with standard errors for both parameters well below 1%. Throughout the entire parameter space, all clouds take their peak mass and peak star mass at the end of the cloud lifetime, just before a dramatic drop in gas content and cloud disruption by feedback. Thus, the peak star mass and gas mass can be combined to a relation which reads

$$\frac{\hat{M}_{\text{S}}}{M_{\odot}} \simeq 1.6 \left( \frac{\hat{M}_{\text{C}}}{M_{\odot}} \right)^{0.58}. \quad (30)$$

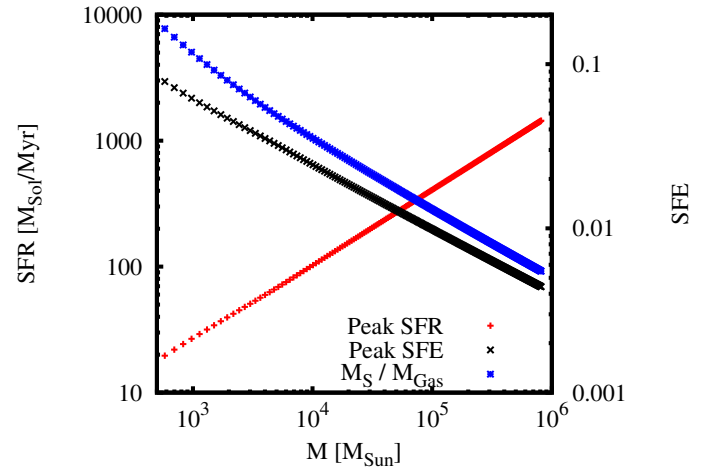


**Fig. 9.** Peak star formation rate, peak star formation efficiency, and peak star mass over peak gas mass plotted as functions of the peak cloud mass. Both the peak SFR and SFE show a simple power-law scaling.

### 5.3. Star formation rates and efficiencies

Figure 9 shows the peak SFR and SFE of clouds with varying peak cloud mass. Both the SFE and the SFR have a power-law scaling. We find that the power laws

$$\frac{\hat{SFR}}{M_{\odot}/\text{Myr}} \simeq 0.40 \left( \frac{\hat{M}_{\text{C}}}{M_{\odot}} \right)^{0.60} \quad (31)$$

and

$$\hat{SFE} \simeq 0.96 \left( \frac{\hat{M}_{\text{C}}}{M_{\odot}} \right)^{-0.40} \quad (32)$$

reproduce the main trends of the plots precisely, with parameter fit errors well below 1%. In all simulations, the SFR increases towards the end of the cloud lifetime resulting in typical age distribution diagrams such as Fig. 10: most stars form just before star formation is terminated. Compared to the Zamora-Avilés et al. (2012) model, we find a similar peak SFR for the  $R_0 = 64$  pc cloud of  $\sim 500 M_{\odot}/\text{yr}$  (see their Fig. 4). For the total number of massive stars, we find a power law

$$N_{\text{OB}} \simeq 0.016 \left( \frac{\hat{M}_{\text{C}}}{M_{\odot}} \right)^{0.58}, \quad (33)$$

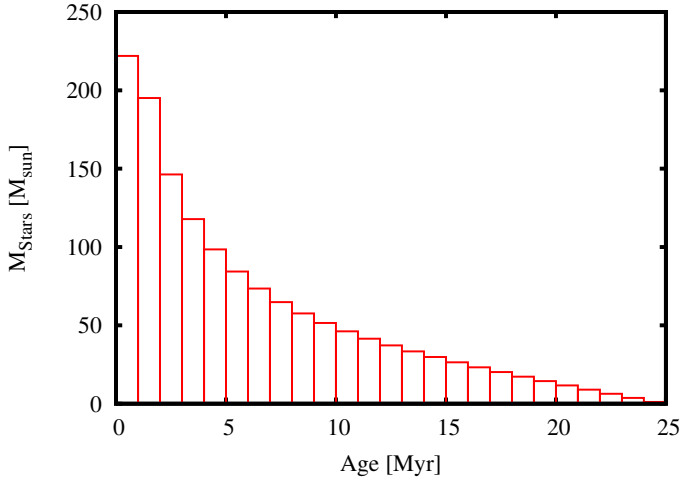


**Fig. 10.** Typical distribution of stellar ages. Here, we selected  $R_0 = 64$  pc as a working example. The SFR peaks at the end of the cloud lifetimes for all clouds in this parameter study. Consequently, most stars are of a young age.

with the smallest clouds forming just one massive star, while clouds with peak masses of  $10^6 M_\odot$  form more than 50 massive stars. Zamora-Avilés et al. (2012) found approximately 100 massive stars for a  $R_0 = 100$  pc cloud. For the same cloud, our model predicts the total number of massive stars that formed over the whole cloud lifetime to be approximately 30.

#### 5.4. Supernova activity

In Fig. 11 we present an overview of the cloud lifetime and supernova activity as predicted by the model. Our model predicts that intermediate-size clouds in the range of  $10^3 M_\odot$  to  $10^4 M_\odot$  feature the shortest life expectancy with a minimum just below 20 Myr, while both larger and smaller clouds live longer lives peaking at 30 Myr. Regarding supernovae, the smallest clouds considered in this parameter study form just enough stars to produce slightly less than one massive star that leaves the main sequence and goes off as a supernova. A result of less than one SN may be interpreted as a supernova probability. More massive clouds, on the other hand, form enough massive stars to see one or more supernovae in the second half of their lifetimes. The most massive clouds of the sample ( $>10^5 M_\odot$ ) see more than 30 supernova explosions, even more massive clouds are likely to see more as they will have greater lifetimes and higher stellar content (cf. Fig. 11).

## 6. Conclusions and discussion

Step by step, we derived the key ingredients to construct a full (semi-)analytical model to describe the dynamical evolution of molecular clouds, the principle stellar nurseries of our universe. At each step, we tried to stick as closely as possible to observations and fundamental astrophysics, and did not introduce any additional efficiencies or parameters.

We started with the global evolution of the cloud, adopting the picture of clouds that can stay in a virialized equilibrium until they start to collapse. The clouds are fed via accretion from two gas streams, but the model does not depend on such an interpretation. Molecular gas forms and is transformed via a star formation criterion that incorporates the idea that the cloud maintains a distribution of cores that follows a Salpeter law. From that,

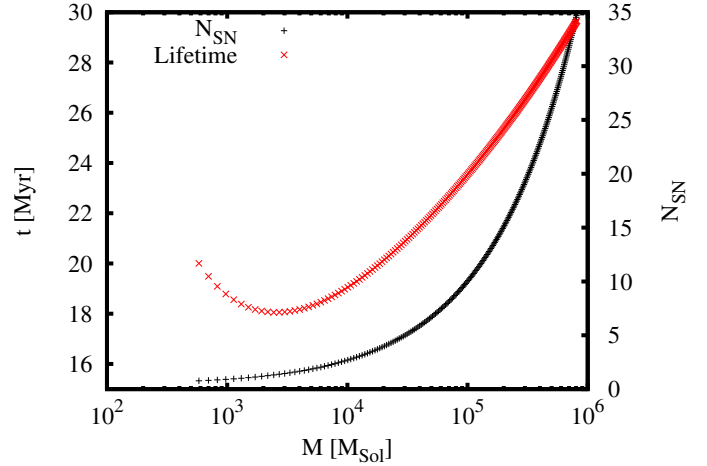


**Fig. 11.** Supernova activity for clouds with varying peak masses. In the model, clouds below a peak mass of  $\sim 10^3 M_\odot$  do not form enough stars and have too short lifetimes to create at least one massive post main sequence star that might blast off as a supernova. Beyond that, more massive clouds are subject to an increasing number of supernovae.

the star forming mass fraction can be determined. Finally, the stars are allowed to feedback with their environment via ionization and supernovae enabling us to calculate evolutionary paths of molecular clouds for a wide variety of cloud sizes. The main results are summarized and compared with other work and observational results as follows.

#### 6.1. Cloud evolution

Molecular clouds evolve over time. Even clouds similar in mass or radius may exhibit different levels of star formation activity simply because they are in different evolutionary phases. This resembles observational results by Kawamura et al. (2009) who defined different stages of molecular cloud evolution.

The typical lifetimes of clouds of sizes between a few parsecs to a few hundred parsecs are 20–30 Myr resembling results by Murray (2011) who found very specific lifetimes of  $27 \pm 13$  Myr. Continuous accretion and star formation delay the collapse and extend the clouds' lifetimes beyond the free-fall time. In addition, small clouds with  $R_0 < 10$  pc can accrete gas for up to 20 Myr before global collapse sets in, representing the fact that smaller clouds are more likely to be found in virial equilibrium (see, e.g., Heyer et al. 2001).

#### 6.2. Star formation

The CMF star formation criterion yields results comparable to established star formation criteria such as Krumholz & McKee (2005) and shows similar scaling with cloud mass and turbulent Mach number. In contrast to the Krumholz model that relies on a number of efficiencies determined by numerical experiments, the CMF criterion incorporates only one observational parameter which is the Salpeter slope. Furthermore, the CMF criterion predicts non-universal star formation threshold densities of the order of  $10^4 \text{ cm}^{-3}$ . Observational studies by various authors (see, e.g., Lada et al. 2010; Pudritz & Kevlahan 2013; Rathborne et al. 2014) confirm that. Regarding turbulence, the CMF criterion is not very sensitive to increasing cloud Mach numbers, showing just a weakly negative scaling. However, it predicts that beyond a certain Mach number, star formation is terminated. The idea that the star formation rate is

simply given as dense gas content over cloud free-fall time (see, e.g., [Krumholz & McKee 2005](#)) results in SFRs in the range 10–1400  $M_{\odot}/\text{Myr}$  for clouds in the range  $10^3$ – $10^6 M_{\odot}$ . A fiducial power law for the gas accretion velocity used in the paper is presented in Sect. 5.3; different values result in slightly different slopes. The predicted SFRs compare well with observational results by [Murray \(2011\)](#) or [Lada et al. \(2010\)](#). For example, they found 715  $M_{\odot}/\text{Myr}$  for *Orion A*, a well evolved GMC with a mass of roughly  $10^5 M_{\odot}$  ([Lada et al. 2010](#)). Younger clouds of comparable mass such as *California* or *Orion B* are characterized by a much smaller stellar content, implying they are in an earlier phase of their evolution. Hence, their star formation rates are much smaller. In principle, the model presented here can be applied to such objects in order to derive an age estimate. Furthermore, all simulations of individual clouds have a star formation rate that increases over time and leads to the typical picture of stellar clusters that are dominated by young stars. That fits the results given by [Palla & Stahler \(2000\)](#) who found that most molecular clouds must have undergone a phase of accelerating star formation to reproduce the stellar cluster age histograms we observe today.

For the smallest clouds, we find star formation efficiencies of up to 10% while the most massive clouds peak at SFEs slightly below 1%. Both the numerical values and the scaling with cloud mass fit observational findings (see, e.g., [Krumholz & McKee 2005](#); [Murray 2011](#)). However, the SFE as employed in this paper also accounts for molecular material that has been destroyed via feedback processes. The naive approach of a star formation efficiency defined as  $M_S/M_C$  leads to doubled values, resembling the observations even better.

### 6.3. Feedback

Within their range of validity, both feedback effects have just a small impact on the evolution of the cloud and decrease the peak star formation rates and efficiencies by only a few percent. Partly, this behavior can be attributed to an inherent limitation of the feedback effects to molecular gas destruction within some given volume fraction of the cloud. Furthermore, we assume those cloud fractions to be filled with mean density molecular gas which does not account for the filamentary structure of molecular clouds and the high density of the star forming cloud parts. As a result, our feedback description may underestimate the overall feedback efficiency and a better description needs to account for the density structure of the cloud as well as the ionized regions (see, e.g., [Franco et al. 2000](#); [Peters et al. 2010b](#)). The energy and momentum input via outflows, stellar winds, and supernovae was neglected in this model, but it may have an effect on the cloud's Mach number and modulate the star formation history once a sufficient number of stars emerged (see, e.g., [Rogers & Pittard 2013](#); [Bally 2016](#); [Padoan et al. 2016](#); [Wareing et al. 2017](#)). On the other hand, our model assumes that all HII regions within the cloud are bound to massive stars which may not hold true depending on the cloud structure and the location of the ionizing star which may lead to higher fractions of ionized gas even up to total cloud ionization (see, e.g., [Franco et al. 1990](#)). For small clouds, our scheme may potentially underestimate the impact of ionization. Apart from photoionization, molecular gas destruction via photodissociation driven by lower-mass stars may serve as an additional feedback effect (see, e.g., [Diaz-Miller et al. 1998](#)).

To conclude, in this model, star formation is regulated neither by turbulence, nor by any stellar feedback effect. Rather, the star formation criterion itself limits the mass that is converted

into stars; feedback processes are only important to limit the lifetime of the cloud. The star formation criterion itself is self-regulating and does not tend to convert clouds entirely into stars even if implemented without competing feedback effects. This result is consistent with the picture of fragmentation induced starvation, that is, a limited star formation efficiency due to fragmentation into subcritical objects ([Peters et al. 2010a](#); [Girichidis et al. 2012](#)).

### 6.4. Conclusions

The (semi-)analytical model presented in this paper agrees well with a large number of observational findings. Molecular cloud evolution can be described by an interplay between accretion, global contraction, star formation, and (modest) feedback effects which can be modeled and understood using basic astrophysics and established astronomical constraints.

*Acknowledgements.* We would like to thank the anonymous referee for helpful comments that improved our manuscript. R.B. and B.K. acknowledge funding for this project by the DFG via the ISM-SPP 1573 grants BA 3706/3-1 and BA 3706/3-2, as well as for the grants BA 3706/4-1 and BA 3706/15-1.

## References

- Adams, F. C., & Laughlin, G. 1997, *Rev. Mod. Phys.*, **69**, 337  
 Bally, J. 2016, *ARA&A*, **54**, 491  
 Banerjee, R. 2014, ArXiv e-prints [[arXiv:1409.7584](#)]  
 Banerjee, R., Klessen, R. S., & Fendt, C. 2007, *ApJ*, **668**, 1028  
 Banerjee, R., Vázquez-Semadeni, E., Hennebelle, P., & Klessen, R. S. 2009, *MNRAS*, **398**, 1082  
 Bertoldi, F., & McKee, C. F. 1992, *ApJ*, **395**, 140  
 Blitz, L., & Shu, F. H. 1980, *ApJ*, **238**, 148  
 Dale, J. E., Ngoumou, J., Ercolano, B., & Bonnell, I. A. 2014, *MNRAS*, **442**, 694  
 Diaz-Miller, R. I., Franco, J., & Shore, S. N. 1998, *ApJ*, **501**, 192  
 Federrath, C., & Klessen, R. S. 2012, *ApJ*, **761**, 156  
 Federrath, C., & Klessen, R. S. 2013, *ApJ*, **763**, 51  
 Federrath, C., Klessen, R. S., & Schmidt, W. 2008, *ApJ*, **688**, L79  
 Federrath, C., Roman-Duval, J., Klessen, R. S., Schmidt, W., & Mac Low, M.-M. 2010, *A&A*, **512**, A81  
 Fierlinger, K. M., Burkert, A., Ntormousi, E., et al. 2016, *MNRAS*, **456**, 710  
 Franco, J., & Cox, D. P. 1986, *PASP*, **98**, 1076  
 Franco, J., Tenorio-Tagle, G., & Bodenheimer, P. 1990, *ApJ*, **349**, 126  
 Franco, J., Kurtz, S., Hofner, P., et al. 2000, *ApJ*, **542**, L143  
 Fukui, Y., Kawamura, A., Wong, T., et al. 2009, *ApJ*, **705**, 144  
 Girichidis, P., Federrath, C., Banerjee, R., & Klessen, R. S. 2012, *MNRAS*, **420**, 613  
 Girichidis, P., Konstandin, L., Whitworth, A. P., & Klessen, R. S. 2014, *ApJ*, **781**, 91  
 Goldreich, P., & Kwan, J. 1974, *ApJ*, **189**, 441  
 Heiles, C., & Troland, T. H. 2003, *ApJ*, **586**, 1067  
 Hennebelle, P., & Chabrier, G. 2008, *ApJ*, **684**, 395  
 Hennebelle, P., & Pérault, M. 1999, *A&A*, **351**, 309  
 Heyer, M. H., Carpenter, J. M., & Snell, R. L. 2001, *ApJ*, **551**, 852  
 Howard, C. S., Pudritz, R. E., & Harris, W. E. 2014, *MNRAS*, **438**, 1305  
 Kawamura, A., Mizuno, Y., Minamidani, T., et al. 2009, *ApJS*, **184**, 1  
 Klessen, R. S. 2000, *ApJ*, **535**, 869  
 Körtgen, B., & Banerjee, R. 2015, *MNRAS*, **451**, 3340  
 Körtgen, B., Seifried, D., Banerjee, R., Vázquez-Semadeni, E., & Zamora-Avilés, M. 2016, *MNRAS*, **459**, 3460  
 Koyama, H., & Inutsuka, S.-I. 2000, *ApJ*, **532**, 980  
 Koyama, H., & Inutsuka, S.-I. 2002, *ApJ*, **564**, L97  
 Kruijssen, J. M. D., Longmore, S. N., Elmegreen, B. G., et al. 2014, *MNRAS*, **440**, 3370  
 Krumholz, M. R., & McKee, C. F. 2005, *ApJ*, **630**, 250  
 Lada, C. J., Muench, A. A., Rathborne, J., Alves, J. F., & Lombardi, M. 2008, *ApJ*, **672**, 410  
 Lada, C. J., Lombardi, M., & Alves, J. F. 2009, *ApJ*, **703**, 52  
 Lada, C. J., Lombardi, M., & Alves, J. F. 2010, *ApJ*, **724**, 687  
 Larson, R. B. 1981, *MNRAS*, **194**, 809  
 Larson, R. B. 1985, *MNRAS*, **214**, 379

- McKee, C. F., & Tan, J. C. 2003, *ApJ*, 585, 850
- Megeath, S. T., Gutermuth, R., Muzerolle, J., et al. 2012, *ApJ*, 144, 192
- Murray, N. 2011, *ApJ*, 729, 133
- Ngoumou, J., Hubber, D. A., Dale, J. E., & Burkert, A. 2014, *Astrophys. Space Sci. Proc.*, 36, 215
- Padoan, P. 1995, *MNRAS*, 277, 377
- Padoan, P., & Nordlund, Å. 2002, *ApJ*, 576, 870
- Padoan, P., Pan, L., Haugbølle, T., & Nordlund, Å. 2016, *ApJ*, 822, 11
- Palla, F., & Stahler, S. W. 2000, *ApJ*, 540, 255
- Peters, T., Klessen, R. S., Low, M.-M. M., & Banerjee, R. 2010a, *ApJ*, 725, 134
- Peters, T., Mac Low, M.-M., Banerjee, R., Klessen, R. S., & Dullemond, C. P. 2010b, *ApJ*, 719, 831
- Pudritz, R. E., & Kevlahan, N. K.-R. 2013, *Phil. Trans. Roy. Soc. Lond. Ser. A*, 371, 20248
- Rathborne, J. M., Lada, C. J., Muench, A. A., et al. 2009, *ApJ*, 699, 742
- Rathborne, J. M., Longmore, S. N., Jackson, J. M., et al. 2014, *ApJ*, 795, L25
- Rogers, H., & Pittard, J. M. 2013, *MNRAS*, 431, 1337
- Salpeter, E. E. 1955, *ApJ*, 121, 161
- Schneider, N., André, P., Könyves, V., et al. 2013, *ApJ*, 766, L17
- Schneider, N., Ossenkopf, V., Csengeri, T., et al. 2015, *A&A*, 575, A79
- Spitzer, L. 1978, *Physical processes in the interstellar medium* (New York: Wiley-Interscience)
- Toalá, J. A., Vázquez-Semadeni, E., & Gómez, G. C. 2012, *ApJ*, 744, 190
- Vázquez-Semadeni, E. 1994, *ApJ*, 423, 681
- Vázquez-Semadeni, E., Ryu, D., Passot, T., González, R. F., & Gazol, A. 2006, *ApJ*, 643, 245
- Vázquez-Semadeni, E., Colín, P., Gómez, G. C., Ballesteros-Paredes, J., & Watson, A. W. 2010, *ApJ*, 715, 1302
- Wannier, P. G., Lichten, S. M., & Morris, M. 1983, *ApJ*, 268, 727
- Wareing, C. J., Pittard, J. M., & Falle, S. A. E. G. 2017, *MNRAS*, 465, 2757
- Zamora-Avilés, M., Vázquez-Semadeni, E., & Colín, P. 2012, *ApJ*, 751, 77
- Zuckerman, B., & Evans, II, N. J. 1974, *ApJ*, 192, L149
- Zuckerman, B., & Palmer, P. 1974, in *BAAS*, 6, 444